Prediction and uncertainty of free convection phenomena in porous media

Yueqing Xie,[1,2] Craig T. Simmons,[1,2] Adrian D. Werner,[1,2] and Hans-J. G. Diersch[3]

Received 30 August 2011; revised 20 January 2012; accepted 25 January 2012; published 29 February 2012.

[1] Over the past few decades, groundwater flow and solute transport models have been commonly used to make predictions of complex, highly nonlinear, semichaotic free convective processes in various hydrogeologic settings. However, there has been much confusion in the literature about the ability of models to make reliable predictions of free convection phenomena. Particularly, different model codes and numerical schemes have been observed to give different solutions to the same problem. Attempts to match the precise nature of finger patterns in space and time have been somewhat unsuccessful. The classical notion of grid convergence appears to be nonmeaningful in the context of these processes when attempting to compare the complex fingering patterns. This study examines the predictability of a highly unstable free convective flow system by quantitatively investigating several representative plume characteristics. These characteristics include "microscopic" features such as the number of fingers and deepest plume front, and "macroscopic" features such as vertical center of solute mass, total solute mass, and solute flux through the source zone. Surprisingly, both microscopic and macroscopic variables can be estimated with a small degree of uncertainty. It is shown that the microscopic variables have slightly greater uncertainty than macroscopic variables. This indicates a greater degree of predictability in free convection systems than may have been previously thought to exist. It also suggests that a paradigm shift which analyses free convection in a stochastic rather than deterministic framework is required. This has significant consequences for model simulation and testing as well as process prediction.

Citation: Xie, Y., C. T. Simmons, A. D. Werner, and H.-J. G. Diersch (2012), Prediction and uncertainty of free convection phenomena in porous media, *Water Resour. Res.*, *48*, W02535, doi:10.1029/2011WR011346.

1. Introduction and Background to Problem

[2] Over the years there has been growing interest in density driven free convection because of its importance in a range of environmental and groundwater contamination issues. It may occur alone or simultaneously with hydraulically driven forced convection. Examples for the occurrence of free convection may include leakage from sanitary landfill sites [*Zhang and Schwartz*, 1995], seawater inundation along coastal aquifers [*Kooi et al.*, 2000], salt accumulation and reflux of saline brines which mix with groundwater in semiarid areas [*Zimmermann et al.*, 2006; *Simmons et al.*, 2002; *Simmons and Narayan*, 1998], and more recently carbon sequestration in deep saline aquifers [e.g., *Han et al.*, 2010]. Recent review articles by *Simmons et al.* [2001], *Diersch and Kolditz* [2002], and *Simmons* [2005] have provided an exhaustive summary on the topic of free convection in porous media and described many of the current challenges in this field of research. Free convective transport is important in groundwater systems because it occurs over larger spatial scales and in shorter time scales compared to diffusion alone. It forms lobe shaped instabilities or fingers and accelerates the spreading of solutes when the density of the invading solute is significantly greater than that of the ambient groundwater. Clearly, carefully evaluating and making reliable predictions about free convective flow can assist us in understanding the mechanisms of free convective transport and taking appropriate measures to reduce and even prohibit environmental problems.

[3] Numerical models have been heavily utilized to investigate free convective transport in groundwater systems due to the difficulty of deriving universal analytical solutions. Conventionally, the ultimate target of exploring free convective transport has been largely focused on obtaining a unique solution of convective patterns and making precise predictions as to the number of fingers, their spatial location, sizes, and migration rates and pathways. However, there has been ongoing failure in attempts across three decades to achieve this goal, and previous work has tended to suggest that free convection may not be easily amenable to prediction. There is strong variability in results of different numerical codes and numerical schemes. The widely studied classic Elder problem [*Elder*, 1967; *Voss and Souza*, 1987] and the salt lake problem [*Wooding et al.*, 1997; *Simmons et al.*, 1999]

[1]National Centre for Groundwater Research and Training, Flinders University, Adelaide, Australia.
[2]School of the Environment, Flinders University, Adelaide, Australia.
[3]DHI-WASY Institute for Water Resources Planning and Systems Research, Berlin, Germany.

0043-1397/12/2011WR011346

are two typical benchmark examples of free convection phenomena that have demonstrated the failure of seeking unique convective patterns in space and time. Despite this, attempts to benchmark codes using these problems persist.

[4] The classic Elder problem was originally established by *Elder* [1967] experimentally and numerically to produce transient thermal convection in a porous layer. It was then transformed into a solute analog convective problem by *Voss and Souza* [1987] for benchmarking the SUTRA groundwater flow and solute transport modeling code. Due to the existence of experimental results, this classic Elder problem has been accepted as one of the primary benchmark models to verify the correctness of numerical codes for simulating variable density flow [e.g., *Diersch and Kolditz*, 2002; *Oldenburg and Pruess*, 1995; *Kolditz et al.*, 1998; *Ackerer et al.*, 1999]. However, numerous studies clearly demonstrated a wide variation in results of converged plume structure, classified into central upwelling and downwelling [*Woods and Carey*, 2007; *Diersch and Kolditz*, 2002], in the classic Elder problem across different numerical codes and numerical schemes. This variability triggered heated debate about the question of which solution is right because this phenomenon was believed to contradict the reproducibility requirement of a benchmark model. Much effort has been dedicated to the quest for the "correct" Elder problem solution, including the application of advanced numerical techniques [e.g., *Frolkovic and De Schepper*, 2001; *van Reeuwijk et al.*, 2009]. Surprisingly, *Frolkovic and De Schepper* [2001] obtained three different steady states at different levels of grid discretization in a grid convergence study in agreement with *Diersch and Kolditz* [2002] and *Johannsen* [2003]. They [*Frolkovic and De Schepper*, 2001] also observed one steady state that occurs at both a coarse grid discretization and a much finer discretization. The study by *van Reeuwijk et al.* [2009] confirmed the existence of multiple solutions of the classic Elder problem—the single (S_1), double (S_2), or triple plume (S_3)—using the pseudospectral method to avoid discretization errors, as demonstrated in Figure 1. This critical result of *van Reeuwijk et al.* [2009] indicates that highly unstable free convective systems are expected to contain multiple solutions and thus a single unique solution is rarely likely. With this in mind, it already begins to seem unreasonable to expect a numerical model to be able to produce a single answer with which code benchmarking can occur. Furthermore, it raises questions about the classical notion of grid convergence and model benchmarking when applied to free convection phenomena, through which multiple solutions are physically plausible.

[5] The salt lake problem [*Wooding et al.*, 1997; *Simmons et al.*, 1999] has also confirmed the difficulty in predicting free convection patterns. The salt lake problem is a complex free convective process involving recharge, evaporation, salt accumulation, and salt reflux in the form of free convection. Inconsistent development of convective patterns was produced in different studies, e.g., *Wooding et al.* [1997], *Simmons et al.* [1999], *Diersch and Kolditz* [2002], *Mazzia et al.* [2001], and *Wooding* [2007]. Particularly, *Mazzia et al.* [2001] concluded that grid convergence in the salt lake problem cannot be achieved due to the sensitivity to numerical errors (i.e., truncation errors) when

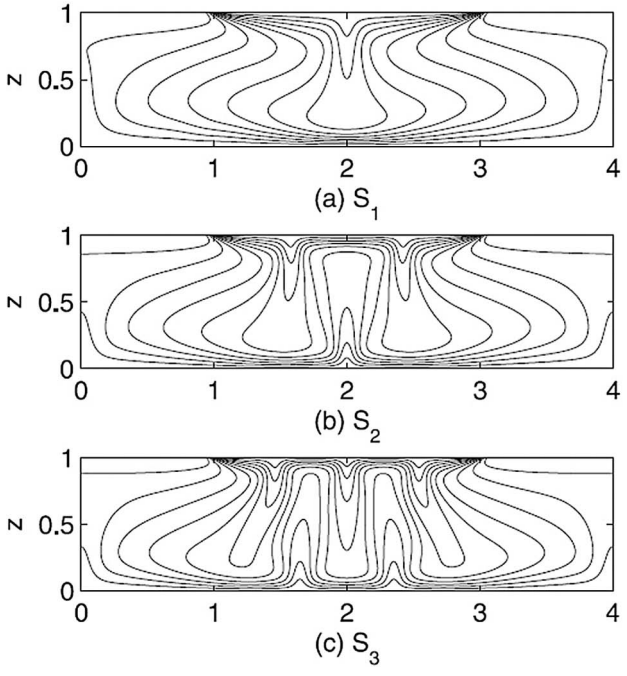

Figure 1. The three steady state solutions of the classic Elder problem at $Ra = 400$ by virtue of various initial conditions. Concentration contours are shown for the single (S_1), double (S_2) and triple plume (S_3) bifurcation solutions [*van Reeuwijk et al.*, 2009]. (Copyright 2009 by the American Geophysical Union. Reproduced by permission of American Geophysical Union.)

they investigated the reliability of the salt lake problem for the verification of numerical codes. *Diersch and Kolditz* [2002] agreed with the difficulty in predicting precise finger number, finger sizes, and descending pathways of fingers.

[6] Earlier work in classical fluid mechanics highlights the nature, complexity and nonlinearity of free convection processes [*Combarnous and Bories*, 1975; *Horne and Caltagirone*, 1980]. *Combarnous and Bories* [1975] summarized the types of free convective behavior in a tilted porous layer with different angles in combination with various values of nondimensional Rayleigh number (*Ra*, Appendix A), as shown in Figure 2. *Ra* is used to indicate the onset of free convection and the degree of instability in porous media. Theoretically, free convection is likely to occur when *Ra* is greater than $4\pi^2$ [*Horton and Rogers*, 1945; *Lapwood*, 1948]. *Combarnous and Bories* [1975] report that a free convection system is characterized by oscillatory and bifurcation behavior when *Ra* exceeds the second critical value (approximately 240–300). It is clear from these results that there are many geometrical configurations for the free convection process. Bifurcations (multiple steady solutions) are well known to exist in classical literature. Moreover, at higher Rayleigh numbers (>240–300) in the oscillatory regime, steady solutions do not occur and free convection is characterized by the continual creation and destruction of cells and fingers.

[7] Free convection in real groundwater systems are often characterized by higher *Ra* values, e.g., $Ra = 400$ in the classic Elder problem [*Elder*, 1967; *Voss and Souza*, 1987], $Ra > 1800$ in a saline disposal basin [*Simmons and*

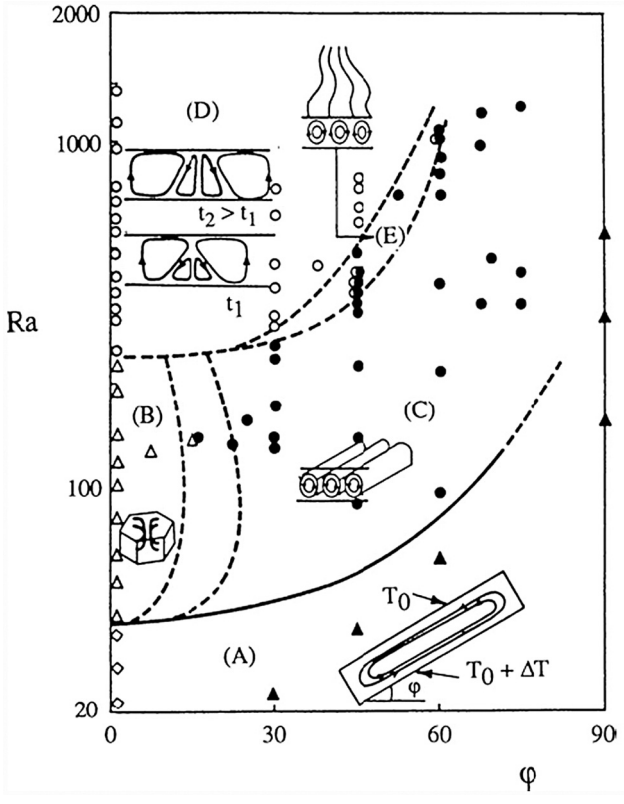

Figure 2. The different types of convective motion experimentally observed in a tilted porous layer: (A) unicellular flow; (B) polyhedral cells; (C) longitudinal stable coils; (D) fluctuating regime; and (E) oscillating longitudinal coils [*Combarnous and Bories*, 1975]. (Copyright 1975 Academic Press.)

Narayan, 1997], $Ra = 4870$ in the salt lake problem [*Wooding et al.*, 1997], and $Ra \approx 5000$ in a tsunami triggered seawater inundation site [*Illangasekare et al.*, 2006]. Clearly free convective groundwater flow is highly unstable with continuous formation and coalescence of fingers [*Diersch and Kolditz*, 2002]. Many free convective groundwater systems are expected to be operating in the oscillatory regime. It also becomes evident that grid convergence of free convection in porous media can almost never be achieved due to the oscillatory and bifurcation behavior, although it might be possible for free convection in fractured rock systems where unstable fingers are restricted in discrete fractures [*Kolditz and Diersch*, 1993; *Graf and Degener*, 2011].

[8] Moreover, free convective systems are extremely sensitive to small perturbations, which are characteristics of natural systems and are uncontrollable in lab or field settings (e.g., pore- or regional-scale heterogeneity in permeability) and in numerical models (e.g., truncation errors and numerical dispersion). Evidently these small perturbations contribute to the difficulty in predicting the behavior of convective cells [e.g., *Schincariol and Schwartz*, 1990; *Schincariol et al.*, 1994; *Simmons et al.*, 1999]. *Schincariol and Schwartz* [1990] reported that they were unable to reproduce instabilities in any laboratory experiments when investigating the variable density flow behavior beneath an injected dense plume in an experimental tank with homogeneous glass beads. *Xie et al.* [2011] explored the descending speeds of unstable fingers using small random perturbations to trigger instabilities along the top boundary in an idealized homogeneous salt lake setting. Their results demonstrate that it is extremely difficult, and probably impossible, to predict the exact size of fingers, the places where fingers form, and their subsequent migration pathways. It is therefore clear that free convection in groundwater systems is essentially a semichaotic process similar to stochastic mechanics and thermodynamics that produces complicated, unpredictable, and seemingly random transient behavior [*Jensen*, 1987].

[9] *Cheng* [1978] compiled several experimental, analytical and numerical results of nondimensional Nusselt number (*Nu*, heat-analogous to Sherwood number, Appendix C) versus *Ra* for thermal convection porous systems heated from below, as demonstrated in Figure 3. *Nu* is the ratio of convective to conductive heat transfer across the source boundary. The studies considered by *Cheng* [1978] employed various boundary conditions, initial conditions, geometrical configurations, and porous media properties. The compilation of data demonstrates that *Nu* is an approximately linear function of *Ra*, although *Nu* values are more scattered with increasing *Ra*. This linear relationship indicates that some macroscopic free convective characteristics (such as heat or salt flux) may well be reliably predicted. The immediate comparison of results from *Combarnous and Bories* [1975] with *Cheng* [1978] suggests that the prediction of free convective processes may indeed be plausible. Despite the widely varying details (e.g., finger number, finger sizes) of the free convection process shown in the work of *Combarnous and Bories* [1975] (what we refer to as the "microscopic" diagnostics of free convection process in this study), there is remarkable predictive power in the relationship shown by *Cheng* [1978] which shows that there is a clear relationship between heat flux and *Ra* (what

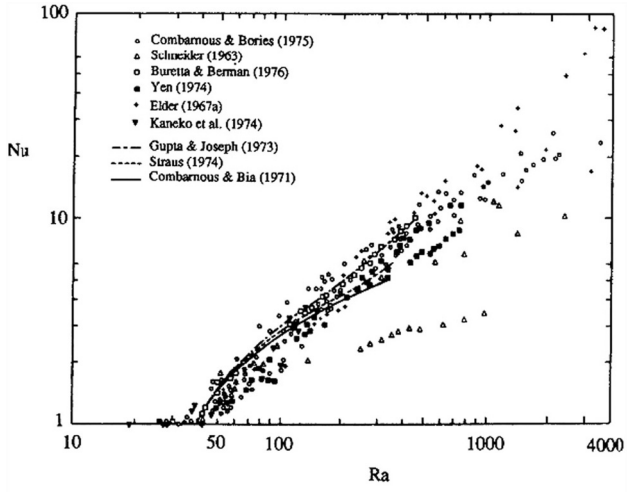

Figure 3. Compilation of experimental, analytical, and numerical results of Nusselt number (*Nu*) versus Rayleigh number (*Ra*) for convective heat transfer in a horizontal layer heated from below [*Cheng*, 1978]. (Copyright 1978 Academic Press.)

we refer to as a "macroscopic" diagnostic of the free convection process in this study).

[10] Some recent studies have adopted various measurable macroscopic diagnostics representing different characteristics (e.g., vertical center of solute mass, total solute mass) to quantitatively analyze variable density flow behavior [*Prasad and Simmons*, 2003, 2005; *Xie et al.*, 2010, 2011]. These studies demonstrate that macroscopic diagnostics are likely to be more reliably predicted under certain circumstances than microscopic ones due to the integrating effect. *Xie et al.* [2011] clearly show that the variability of both the descent of the vertical center of solute mass and plume front movement is very small. They also report that the descent of the vertical center of solute mass can be more reliably predicted than plume front movement, as indicated by a three-fold difference in the variability obtained from stochastic simulations. *van Reeuwijk et al.* [2009] adopted the Sherwood number (*Sh*, a nondimensional quantity to measure the ratio of total solute flux to pure diffusive flux across the source zone) to quantitatively distinguish the three steady state solutions that are physically plausible in the classic Elder problem—the single (S_1), double (S_2), or triple plume (S_3) as shown in Figure 4. At $Ra = 400$, three physically plausible steady state solutions are possible. Despite this, there is less than 25% variability in the *Sh* number for the three different solutions. This result indicates the possibility of reasonable solute flux prediction capability in free convective behavior despite the three different fingering configurations, consistent with the earlier discussion associated with *Combarnous and Bories* [1975] and *Cheng* [1978].

[11] Although there is increasing interest in the use of different measurable diagnostics, whether free convection can be reliably predicted is not clear and the objective quantitative assessment of the predictability of free convective transport is lacking in existing literature.

[12] This introductory material raises some key questions: What is our quantitative ability to predict the different features (both macroscopic and microscopic) of the free convection process? What is the inherent uncertainty in those predictions? Is it still necessary to compare precise finger details in space and time? Do we need to alter our expectations from grid convergence and model benchmarking exercises? Can we continue to make deterministic assessments in free convection systems which are highly nonlinear and hence ultimately may necessarily lend themselves far better to stochastic assessment?

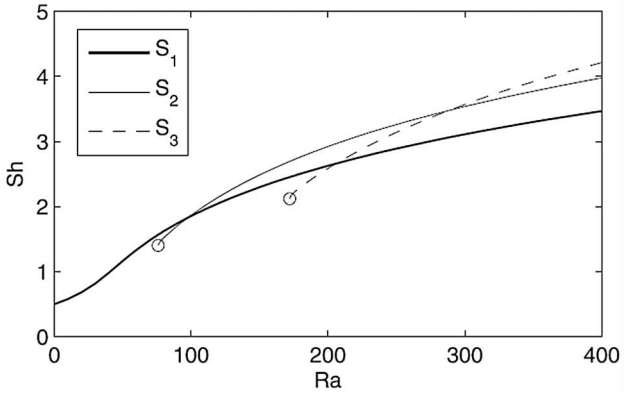

Figure 4. Bifurcation solutions of the classic Elder problem for $0 < Ra < 400$. The bifurcations are evident in the different Sherwood number (*Sh*) for each solution [*van Reeuwijk et al.*, 2009]. (Copyright 2009 by the American Geophysical Union. Reproduced by permission of American Geophysical Union.)

[13] This study aims to systematically and quantitatively assess predictive capability and associated uncertainty in the simulation of free convective processes. This assists us to answer the questions raised above. The highly unstable free convection problem used previously by *Xie et al.* [2011] is adopted to serve as a base case, and five measurable diagnostics including number of fingers, deepest plume front, vertical center of mass, total mass of solute, and *Sh* are quantified to provide rigorous examination, in combination with visual inspection of convective patterns.

2. Numerical Experiments

[14] In this study we adopted the free convection problem employed by *Xie et al.* [2011] to explore the predictability of free convective fingering in fully saturated homogeneous and isotropic porous media. This free convection system was modified from the classic solute-analogous Elder problem [*Voss and Souza*, 1987] to be more representative of natural free convection in porous media. The features of this free convection system include: (1) it is relevant to natural salt lake settings [e.g., *Van Dam et al.*, 2009] due to its high density of the salt source (i.e., 1200 kg m^{-3}) placed along the entire top of the system; (2) it is a dispersive system using reasonable longitudinal and tranverse dispersivities of 1 m and an appropriate molecular diffusivity (2.8×10^{-9} m^2 s^{-1}) for solute transport, to replace the high value (3.565×10^{-6} m^2 s^{-1}) originally representing the thermal diffusivity in the heat-analogous Elder problem [*Elder*, 1967]; (3) the opportunity of aquifer-scale circulations causing centralizing phenomena is minimized after the solute source was extended to the entire top boundary; (4) the computational burden is reduced after the system was resized to a smaller fully saturated square aquifer (100 m $\times$ 100 m); and (5) this free convection system is highly unstable and is characterized by a *Ra* of 3.4×10^5. We have deliberately picked a very unstable case instead of those less unstable benchmark models like the Elder problem and the salt lake problem to examine in this study, i.e., highly oscillatory and chaotic convection is expected at this very high *Ra* number. This *Ra* number may be considered somewhat of a worst case scenario for the case of a homogeneous and isotropic porous media setting. The conceptual model is presented in Figure 5 and the fluid and matrix parameters are listed in Table 1.

[15] The spatial and temporal discretization was chosen to minimize numerical dispersion since grid convergence is unlikely to be achieved [*Mazzia et al.*, 2001]. We used the common criterion mesh Peclet number $Pe \approx \Delta L/\beta_L < 2$ [*Diersch and Kolditz*, 2002], where ΔL is the transport distance between two sides of an element measured in the direction of groundwater flow [*L*] and β_L is the longitudinal dispersivity [*L*], to guide grid disretization. We also utilized two macroscopic diagnostics (i.e., deepest plume front and vertical center of solute mass) to quantify and compare free

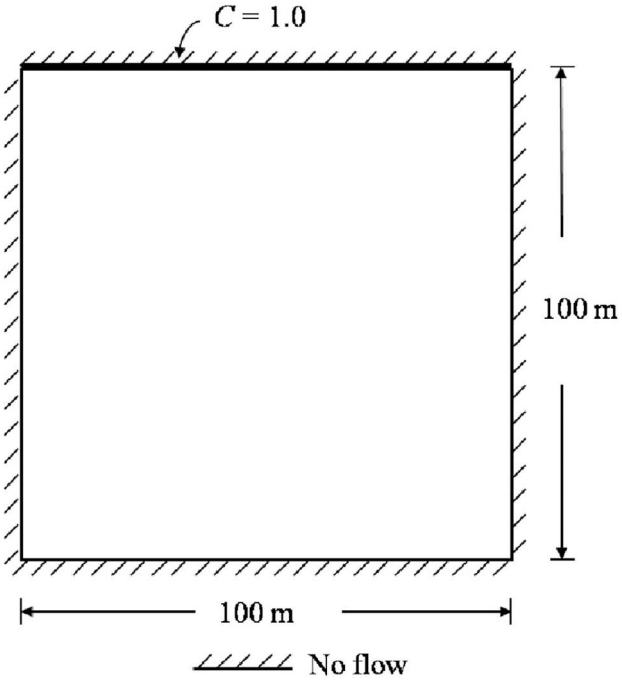

Figure 5. The geometry and boundary conditions of the conceptual model adopted from *Xie et al.* [2011].

convective behavior at different levels of discretization. Preliminary results showed that those diagnostics demonstrated about the same growth rates in speed as at finer discretizations using a grid comprising 176,000 elements and 179,376 nodes, with maximum $Pe = 0.25$, $\Delta x = 0.25$ m ($0 < x < 100$ m), $\Delta y = 0.125$ m ($0 < y < 10$ m) and $\Delta y = 0.25$ m ($10 < y < 100$ m), where Δx and Δy are the element length and height [L], respectively.

[16] The finite element subsurface groundwater flow model FEFLOW (H. J. G. Diersch, FEFLOW: Finite Element Subsurface Flow and Transport Simulation System, WASY GmbH Institute for Water Resources Planning and Systems Research, 2005) was employed to simulate the groundwater flow and solute transport. Fluid, solute, and momentum conservation equations are given in Appendix B. We always used highly refined meshes in the Galerkin-based finite element analysis without any resort to upwind schemes. For the spatial two-dimensional discretizations bilinear four-noded quadrilateral elements are applied. Furthermore, an adaptive predictor-corrector time stepping technique is preferred with the Adams-Bashforth scheme as predictor and the trapezoid rule as corrector which is second order accurate in time. The temporal error control is combined with a one-step Newton method to accelerate convergence. Constraints of the initial time step of 10^{-8} days and time step limit of 1 day are adopted. To ensure higher accuracy in the derived velocities for variable-density flow, a consistent approximation using the Frolkovic-Knabner algorithm has been employed. A local smoothing procedure is applied to derive continuous nodal velocities. All these numerical techniques are thoroughly discussed by *Diersch and Kolditz* [1998, 2002] and have proved to be accurate and reliable numerical schemes for the present class of variable density flow. The total simulation time is 10 years, which allows the vertical center of mass to stabilize at around the vertical center of the system. The runtime of each realization in FEFLOW is around 10 h using this spatial and temporal discretization on a Dell Precision T3400 Tower Workstation.

Table 1. Simulation Parameters for the Conceptual Model

Parameter	Symbol	Value	Unit
Model length	x	100	m
Model height	y	100	m
Element length	Δx	0.25	m
Element height	Δy	0.125 ($0 < y < 10$ m) 0.25 ($10 < y < 100$ m)	m
Permeability	k	4.845×10^{-13}	m^2
Effective porosity	ε	0.1	–
Longitudinal dispersivity	β_L	1.0	m
Transverse dispersivity	β_T	1.0	m
Molecular diffusivity	D_0	2.8×10^{-9}	$m^2\ s^{-1}$
Dynamic viscosity	μ	1.0×10^{-3}	$kg\ m^{-1}\ s^{-1}$
Freshwater density	ρ_0	1000	$kg\ m^{-3}$
Gravitational acceleration	g	9.81	$m\ s^{-2}$
Density contrast ratio	$\overline{\alpha}$	0.2	–
Specific Storage	S_S	1.0×10^{-8}	m^{-1}
Initial freshwater head throughout	$h_{initial}$	0	m
Initial concentration throughout	$C_{initial}$	0.0	–
Scaled concentration at the top boundary	C_{top}	1.0	–

[17] *Xie et al.* [2011] adopted a random perturbation function in the form of small spatiotemporal variations in concentration, to trigger instabilities at the boundary layer. The perturbation is intended to represent the variability inherent in natural systems, e.g., due to such factors as irregularity in evaporation, local-scale heterogeneity in hydraulic conductivity [*Simmons et al.*, 1999; *Post and Simmons*, 2010], and so on. The use of perturbations follows *Horne and Caltagirone*'s [1980] suggestion that small random perturbations should be introduced into nonlinear problems to represent system noise and perturb otherwise perfect mathematical equations. They specifically noted "*It is perhaps time to admit that mathematical solutions to nonlinear problems must of necessity include nondeterministic forcing effects in order to avoid solutions mathematically correct but physically unlikely.*" This early work suggested the need for a stochastic approach to the solution of free convection problems, but this advice has been largely ignored to date.

[18] The perturbation function is adopted from *Simmons et al.* [1999] and is given by

$$C_{node} = C_{dense} + \frac{1}{100}(C_{dense} - C_0)(\text{rand}\,(0) - 0.5), \qquad (1)$$

where C_{node} is the normalized concentration of any single node at the top [–]; C_{dense} and C_0 are the normalized concentration of dense water and freshwater, respectively [–]; rand (0) is a random function used for generating random and uniformly distributed numbers between 0 and 1 [–]. The concentration boundary condition along the top was only perturbed once before the simulation started and remained unchanged afterwards. This was conducted to observe the influence of initial perturbation on free convective fingering behavior. Note that preliminary results do not show any significant difference in simulation results

from time-dependent random perturbations. In addition, we performed a series of simulations to examine the potential influence from various perturbation amplitudes (0%, 0.5%, 1%, and 2%). Preliminary results suggest that this current perturbation amplitude (0.5%) is sufficiently small and reasonable to perturb fingers at early stages without causing strong impact on fingering process at later stages.

[19] The incorporation of the random perturbation function clearly exacerbates the range of bifurcation solutions that may be physically plausible. This meanwhile enables us to run stochastic numerical simulations which produce statistical results (mean μ and standard deviation σ) to interpret the predictability and uncertainty of free convection. μ demonstrates the overall trends of each diagnostic and σ indicates the corresponding variability. In accordance with the central limit theorem in the probability theory [*Kreyszig*, 1988], the distribution of a sampling will become Gaussian or nearly Gaussian once the size of the sampling is sufficiently large. The Gaussian distribution of any variable can yield a confidence interval of $\pm 3\sigma$ at a confidence level of 99.7%. The rule-of-thumb minimum sampling size required to establish a Gaussian distribution is 30. Therefore, similar to *Prasad and Simmons* [2003], this model was simulated 30 times with small random perturbations to analyze the predictability and uncertainty of free convection. Note that we do not perform more simulations to ensure the convergence of the distribution because it is computationally prohibitive and expensive, and hence we cannot guarantee the convergence of the statistic results from this suite of stochastic simulations. Despite this, the principle and the corresponding results are not expected to change significantly if more simulations are conducted.

[20] Five measurable diagnostics were used to quantify different characteristics of the free convection system (as well as visual inspection throughout space and time), including number of fingers (NOF), deepest plume front (DPF), vertical center of mass (COM), total mass of solute (TM) and Sherwood number (*Sh*). NOF is identified through automatically counting the number of finger tips using the relative solute concentration of $C = 0.01$. DPF is the depth of the deepest finger tip using $C = 0.01$ and measured from the top. COM is the integrated vertical center of mass of the salt plume across the entire model domain and measured from the top. *Sh* is the spatially integrated salt flux along the top concentration boundary condition. Clearly, NOF and DPF are microscopic diagnostics and COM, TM, and *Sh* are macroscopic diagnostics according to their definitions. These diagnostics are intended to capture both small scale and larger scale characteristics of free convection phenomena, considering both microscopic and macroscopic perspectives of the predictability and uncertainty of free convection. Detailed mathematical definitions of diagnostics are given in Appendix C. We acknowledge that there may be other measurable characteristics which may reflect other characteristics of free convection.

3. Results

3.1. Qualitative Inspection

[21] Figure 6 qualitatively compares the fingering behavior of two realizations at different simulation times. Finger

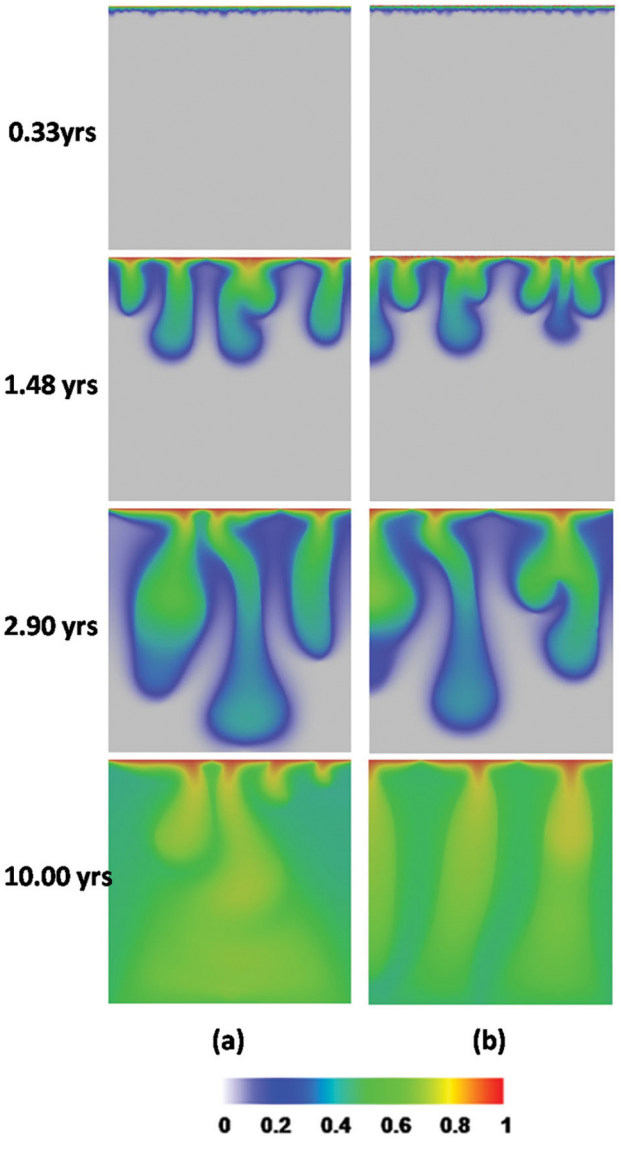

Figure 6. Finger patterns from two realizations at four different times. Despite the difference in finger patterns, finger penetration rate, and finger number are comparable between (a) and (b).

patterns are clearly different between realizations at all times throughout the model runs, whereby unstable fingers are not expected to form at the same places. For example, the progression of an unstable finger abutting the left boundary in Figure 6b does not occur in Figure 6a (due to variations in the upward flow of fresh groundwater in response to downward density-driven flow). Clearly, exact convective patterns are impossible to reproduce due to the sensitivity to perturbations (both added boundary perturbations and inherent system noise of truncation errors) in agreement with *Schincariol and Schwartz* [1990].

[22] It is initially tempting to conclude that the precise details of the fingers cannot be matched. However, a closer inspection of these different fingering patterns suggests that there are qualitative similarities in finger characteristics. The deepest finger tip is seen to move downward at

relatively similar speeds before reaching the bottom of the domain (e.g., compare the deepest finger tips in two realizations at 1.48 years and 2.90 years, respectively). In addition, the number of fingers appears to be on the same order at all times in both realizations. For instance, there are five and seven fingers, respectively, at 1.48 years; three and four fingers, respectively, at 2.90 years. Clearly both quantifiable finger characteristics (speed of fingers and number of fingers) are more likely to be appropriately predicted than finger locations and pathways. All of these characteristics are obviously sensitive to small perturbations—not only those which are physically applied to the model in the concentration boundary but also numerical errors and numerical dispersion inherent to the numerical methods employed. It can then be inferred that those characteristics of free convection which are spatially integrated are more likely to be predicted with greater accuracy in an unstable free convection system.

3.2. Quantitative Analysis

[23] Figure 7 shows the development of μ and σ for four measurable diagnostics (i.e., NOF, DPF, COM, and *Sh*) derived from the stochastic numerical simulations. μ illustrates the time-varying trends in different finger characteristics, whereas σ demonstrates the corresponding variability. The maximum and minimum values of diagnostics are superimposed in all subgraphs for illustrative purposes. Note that the observation of NOF and DPF was terminated once DPF reached the system bottom, whereas the monitoring of COM and *Sh* was conducted throughout the entire model simulation.

[24] Three stages are apparent in the time-varying behavior of μ. In the first stage (from the commencement to approximately 0.5–1 year), the boundary layer was progressively established and unstable fingers were slowly generated. μ(DPF), μ(COM), and μ(*Sh*) are seen to gradually accelerate due to the development and subsequent coalescence of unstable fingers. μ(NOF) clearly demonstrates the rapid decrease in finger numbers resulting from finger coalescence. In comparison, σ(DPF), σ(COM), and σ(*Sh*) increase, whereas σ(NOF) decreases to a relatively stable level. σ values are relatively small compared to μ values despite various temporal trends in μ. This indicates that free convection can be well predicted during this stage. In the second stage (the end of the first stage to around 3–4 years), unstable fingers started to descend vigorously before reaching the bottom of the free convection system. Although μ values demonstrate steady (close to linear) variation with time during this stage, the variability in diagnostics (i.e., σ) is enhanced due to the strong circulations associated with free convection. Therefore the prediction about free convection during this stage becomes more difficult. This is also evidenced by the increasing distances between maximum and minimum values of each diagnostic. At the final stage,

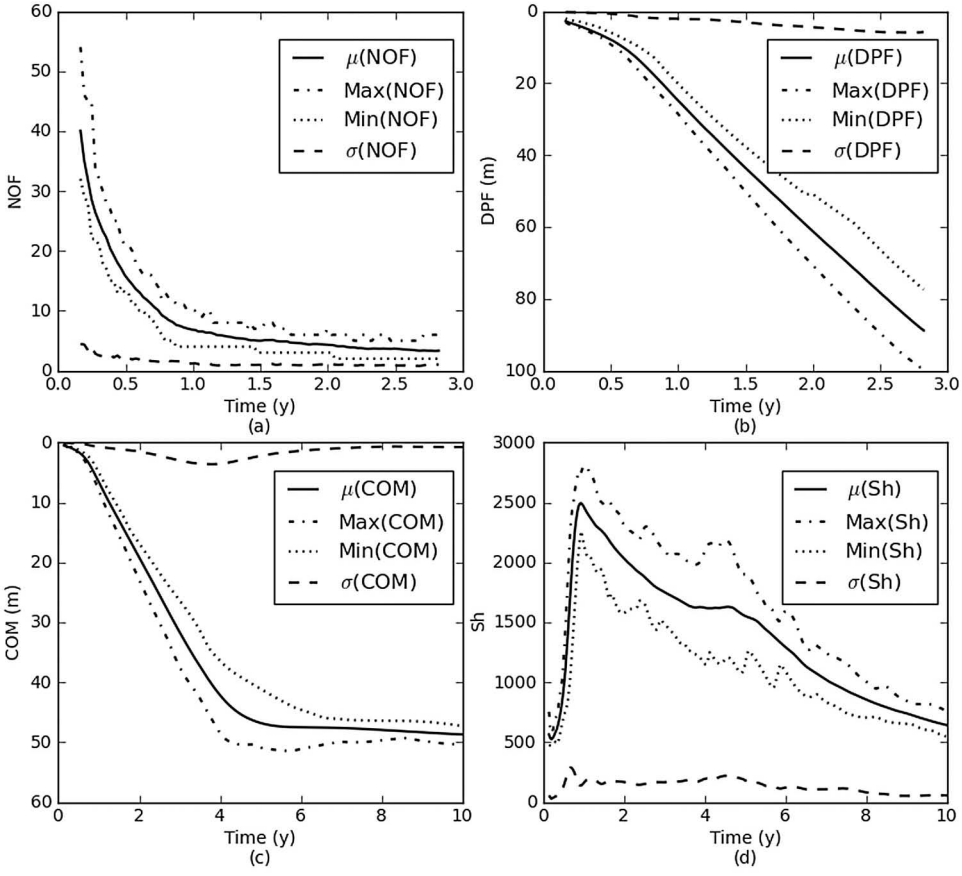

Figure 7. The evolution of statistical features (mean μ and standard deviation σ) of four measurable diagnostics with time. The maximum and minimum values of all diagnostic variables are also plotted for comparison.

salt started to fill up the system and to subsequently cause the reduction of density difference which obviously weakened the strength of free convection. Figures 7c and 7d demonstrate the behavior of COM and *Sh* at the final stage. It is seen that μ(COM) asymptotes to the vertical center of the system (50 m) and μ(*Sh*) continues to drop in response to the salt accumulation. The corresponding σ(COM) and σ(*Sh*) are seen to decrease due to the resultant decline in fingering dynamics. The decrease in σ(COM) and σ(*Sh*) suggest that free convection starts to have much better predictability again.

[25] Figure 8 illustrates the variation in the coefficient of variation (CV) of all measurable diagnostics in order to reflect the uncertainty of free convective behavior. CV is defined as the ratio of σ to μ and may be thought of as the inverse of a signal-to-noise ratio. A large CV value is therefore problematic from a prediction and uncertainty point of view, whereas small values imply a strong signal with small noise and hence good predictive power. Furthermore, since CV is a dimensionless number, it is a useful way to compare data sets with different units or widely different means [e.g., *Larocqueet al.*, 2009]. Figure 8 shows that all macroscopic diagnostics (COM, *Sh*, and TM) and one microscopic diagnostic (DPF) have highest uncertainty around the time that fingers formed along the boundary layer and started to coalesce into large structures. After unstable fingers reached the bottom, COM and TM presented very small uncertainty (CV $<$ 0.05) compared to the uncertainty of *Sh* which fluctuates around 0.1. By contrast, the uncertainty of NOF increases up to 0.31 while heavily fluctuating. This is mainly attributed to the nature of this diagnostic which is strongly sensitive to oscillatory and bifurcation behavior. While it is clear that macroscopic variables are less uncertain and hence more predictable than their microscopic counterparts, all variables (whether microscopic or macroscopic) are actually able to be reliably predicted based on overall small CV values for all diagnostics employed in this study.

[26] It is worth noting that a comparison has been done by *Xie et al.* [2011] to examine potential influence from different geometrical domain sizes, random perturbation amplitudes, and discretization schemes. Their results indicate that a change in each aspect may cause finger details (e.g., number of fingers, individual finger locations, and finger patterns) to vary, but may not lead to significant variation in measurable variables.

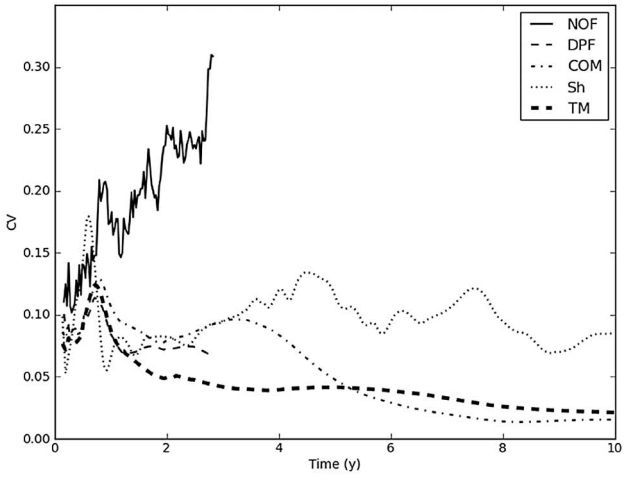

Figure 8. The development of the coefficient of variation (CV) of all diagnostics used in this study.

4. Discussion

[27] The results above show that both the convective patterns and the measurable characteristics of an extremely unstable free convective flow system are unlikely to be reproduced in exact terms through numerical simulation, in agreement with the findings of others [e.g., *Mazzia et al.*, 2001]. The density effect leads to strong sensitivity of the free convective system to external controllable perturbations (i.e., the random physical perturbations applied to the top source zone) and internal uncontrollable noise (i.e., numerical perturbations arising from truncation errors). Moreover, the real-world free convective systems are much noisier than numerical models as perturbations exist everywhere in the form of different heterogeneities, e.g., nonuniform evaporation, concentration variation of intruding contaminant plumes, porescale, or regional-scale heterogeneity in permeability distribution, etc. Therefore, it is impossible to reproduce the finger patterns in practical experiments and field situations, as pointed out by many earlier authors [e.g., *Bachmat and Elrick*, 1970; *Schincariol and Schwartz*, 1990]. It is also unreasonable to expect that one numerical solution would exist and that this solution would form the basis for both grid convergence tests and other model benchmarking exercises.

[28] This study suggests that variables (NOF, DPF, COM, *Sh*, and TM) are highly predictable and span both macroscopic and microscopic diagnostics. Considering the inherently unstable characteristic of the chaotic free convection studied here, the uncertainties (i.e., CV $<$ 0.31) are not only reasonable and acceptable from a prediction/uncertainty viewpoint, but also much smaller than may be intuitively expected. This suggests that many aspects of the free convection process may be amenable to prediction when viewed in a stochastic framework, i.e., we should not expect to match the precise number of fingers and the precise spatial and temporal features of a fingering pattern, but we can still make inferences that are meaningful about the behavior of the free convection process. We therefore contend that free convective behavior can be better understood and predicted through quantitative analysis of measurable diagnostics rather than solely relying on qualitative inspection of convective patterns and matching concentration isochlors in space and time. Considering high *Ra* of 3.4×10^5 in this study, better prediction capability is expected at even lower *Ra*.

[29] It is necessary to compare the uncertainty of free convective characteristics with the uncertainty of hydraulic conductivity (*K*) that significantly affects unstable plume development as identified by *Post and Kooi* [2003] and *Xie et al.* [2011]. It is commonly recognized that *K* may vary over several orders of magnitude [*Freeze and Cherry*, 1979], despite that numerous techniques are developed to better interpret the hydraulic testing data from field tests [*Renard*, 2005]. Even in a homogeneous setting, it is rare to be able to constrain *K* to within an order of magnitude. Therefore, there is a factor of 10

variability in all predicted results due to the uncertainty of K. In comparison, given the fact that CV < 0.31, there is only a factor of 2 variability in results using $\mu \pm 3\sigma$ for the confidence level of 99.7%. Ultimately our ability to make sensible predictions about free convection appears to be rate limited by our ability to make sensible predictions about K. Note that these results only apply to a homogeneous and isotropic field setting. The situation is far more complex in heterogeneous geologic settings as has been highlighted by prior studies [e.g., *Simmons et al.*, 2001; *Simmons et al.*, 2010; *Nield and Simmons*, 2007; *Prasad and Simmons*, 2003; *Schincariol*, 1998] where the nature of the heterogeneity controls the onset, growth, and decay of free convective instabilities.

[30] This study demonstrates that the simulation and hence prediction of free convection processes requires a stochastic way of thinking instead of deterministic thinking. This has profound consequences for what we can reasonably expect for model testing, benchmarking, and grid convergence and a radically different way of approaching the problem. For example, rather than counting the precise number of fingers and comparing them precisely in space and time (a deterministic model test based on the assumption of a single realization which we clearly know is incorrect), we expect that the new paradigm will consider model testing within a stochastic framework and compare means and standard deviations of the models across multiple realizations for various microscopic variables. This stochastic framework is particularly required to investigate dense plume migration in heterogeneous permeability fields [*Schincariol*, 1998] because it is impossible to quantify the details of local-scale permeability distributions which may act as unknown random perturbations.

[31] Some contextualizing comments on this work are now useful. The paper is an attempt to open a pathway to new thinking in the water resources community when dealing with free convection processes. The message in this paper is therefore one which may reach both researchers and practitioners in this discipline of hydrogeology. There has been much discussion on the problems faced when modeling unstable free convection in the water resources community in recent years, some of which is captured in the introduction to this paper. We hope this current work provides the opportunity for a new discussion in order to give a more enhanced orientation in future research and applications for free convection phenomena. We draw some parallels here with turbulent fluid modeling, despite the obvious differences in the physics of these phenomena. In current turbulent fluid dynamics today, very few people are trying to model exactly and count single eddies. There are, however, some exceptions which have an academic orientation at very low Reynolds numbers in a fully laminar flow regime. We observe that, in contrast, averaged and macroscopic quantities are always accepted and applied in the discipline of turbulent fluid mechanics. The conclusions of this work should not be interpreted as a need to move from detailed modeling to rough modeling, but rather a recognition of the physics of instability processes. Indeed, detailed and robust modeling is a necessary precursor to ensure that the numerical solutions obtained are indeed a part of the ensemble of physically plausible solutions and are not numerically spurious. This detailed modeling and the range of physically plausible solutions then forms the basis for appropriate averaging and the determination of macroscopic quantities.

5. Conclusions

[32] This study has systematically and quantitatively investigated the predictability of free convective groundwater flow in an idealized homogeneous and isotropic porous medium using a perturbation-based stochastic model. Several measurable characteristics were selected to examine both microscopic and macroscopic aspects of the predictability of convective instabilities as well as visually inspecting the unstable convective patterns. These characteristics included microscopic diagnostics (NOF, DPF) and macroscopic diagnostics (COM, TM, and *Sh*). All diagnostics have displayed different levels of variability and have therefore confirmed the difficulty in achieving exact reproducibility of free convective behavior, consistent with previous studies [*Bachmat and Elrick*, 1970; *Schincariol and Schwartz*, 1990; *Mazzia et al.*, 2001]. However, given the complexity of free convection (i.e., oscillatory and bifurcation behavior due to high Ra of 3.4×10^5), the demonstrated variability of all diagnostics is surprisingly small and reasonable (CV < 0.31). We therefore contend that free convective behavior can be more reliably predicted through quantitative stochastic analysis of measurable diagnostics than qualitative inspection of convective patterns.

[33] It is also probably the time to require a paradigm shift in regards to research on free convective processes. We should consider macroscopic variables as effective tools instead of microscopic finger details to quantify finger movement. We should also start to think and work stochastically rather than deterministically to acknowledge the physical nature of free convection process (multiple bifurcation solutions and oscillatory solutions) and hence makes stochastic (and not deterministic) assessments and comparisons of free convective processes within and between numerical models.

[34] Clearly further work is required to assess this within other free convection problems that are routinely employed as benchmarks, but the work here highlights a novel pathway forward for this field which has not been routinely adopted to date. This is based on drawing critical links between pertinent literature in this topic but also through the quantitative assessment presented in this study.

Appendix A: Rayleigh Number

[35] The dimensionless Rayleigh number Ra is an indicator of the onset of instabilities in this system and is given by:

$$Ra = \frac{k\rho_0 g \overline{\alpha} H}{\mu \varepsilon D_0}, \tag{A1}$$

where k is intrinsic permeability; g is acceleration due to gravity, $\overline{\alpha} = (\rho - \rho_0)/\rho_0$ is the density contrast coefficient, ρ_0 is base reference fluid density, ρ is fluid density, H is the vertical extent of the flow regime, μ is dynamic viscosity, ε is effective porosity, and D_0 is the aqueous molecular diffusion coefficient.

Appendix B: FEFLOW Governing Flow and Transport Equations

[36] The governing equations in FEFLOW (H. J. G. Diersch, FEFLOW: Finite Element Subsurface Flow and Transport Simulation System, WASY GmbH Institute for Water Resources Planning and Systems Research, 2005) are composed of fluid mass, momentum, and solute mass conservation equations.

[37] Fluid mass conservation equation is given by

$$\frac{\partial(\varepsilon\rho)}{\partial t} + \nabla\cdot(\varepsilon\rho\mathbf{v}) = \varepsilon\rho Q_\rho, \tag{B1}$$

where $\mathbf{v}$ is pore (intrinsic) velocity and Q_ρ is the fluid mass source/sink. It is assumed that density is linearly proportional to concentration:

$$\rho = \rho_0\left(1 + \frac{\overline{\alpha}}{C_s - C_0}(C - C_0)\right), \tag{B2}$$

where C is the normalized concentration, C_0 is the normalized base reference concentration, and C_s is the normalized maximum concentration.

[38] Momentum conservation equation (i.e., Darcy's law) is given by

$$\mathbf{v} + \frac{\mathbf{k}}{\varepsilon\mu}\cdot(\nabla p - \rho\mathbf{g}) = 0, \tag{B3}$$

where p is fluid pressure.

[39] Solute mass conservation equation is given by

$$\frac{\partial(\varepsilon C)}{\partial t} + \nabla\cdot(\varepsilon C\mathbf{v}) + \nabla\cdot j = Q_c, \tag{B4}$$

where Q_c is the solute mass source/sink. j is Fickian mass flux governed by Scheidegger-Bear's dispersion approach:

$$j = -\varepsilon\left[(D_0 + \beta_T\|\mathbf{v}\|)\boldsymbol{I} + (\beta_L - \beta_T)\frac{\mathbf{v}\otimes\mathbf{v}}{\|\mathbf{v}\|}\right]\cdot\nabla C. \tag{B5}$$

[40] β_L and β_T are the longitudinal dispersivity and transverse dispersivity, respectively, $\boldsymbol{I}$ is the unit (identity) tensor.

Appendix C: Mathematical Definitions of Diagnostics

[41] The dimensionless Sherwood number (Sh) is the ratio of the actual transfer rate of solute mass due to free convection to the transfer rate of solute mass due to diffusion, and is given by

$$Sh = \frac{mH}{WL_sD_0\Delta C}, \tag{C1}$$

where m is the mass flux across the source boundary, W is the width of the source zone and is equal to unity for the cross-sectional layout of the domain, L_s is the length scale of the source zone, and ΔC is the maximum concentration difference between base reference concentration and maximum concentration.

$$\mathrm{COM} = \frac{1}{\mathrm{TM}}\int \rho(y)y\,dV, \tag{C2}$$

where TM is the total solute mass and $\rho(y)$ is the integral density at the depth y.

[42] The mean and standard deviation of Sh are given by

$$\mu(Sh) = \frac{\sum_{i=1}^{n}(Sh)_i}{n}, \tag{C3}$$

$$\sigma(Sh) = \sqrt{\frac{\sum_{i=1}^{n}[(Sh)_i - \mu(Sh)]^2}{n-1}}, \tag{C4}$$

where n is the number of samples in a set of models. $n = 30$ in this study.

[43] The mean and standard deviation of NOF are given by

$$\mu(\mathrm{NOF}) = \frac{\sum_{i=1}^{n}(\mathrm{NOF})_i}{n}, \tag{C5}$$

$$\sigma(\mathrm{NOF}) = \sqrt{\frac{\sum_{i=1}^{n}[(\mathrm{NOF})_i - \mu(\mathrm{NOF})]^2}{n-1}}, \tag{C6}$$

[44] The mean and standard deviation of DPF are given by

$$\mu(\mathrm{DPF}) = \frac{\sum_{i=1}^{n}(\mathrm{DPF})_i}{n}, \tag{C7}$$

$$\sigma(\mathrm{DPF}) = \sqrt{\frac{\sum_{i=1}^{n}[(\mathrm{DPF})_i - \mu(\mathrm{DPF})]^2}{n-1}}. \tag{C8}$$

[45] The mean and standard deviation of COM are given by

$$\mu(\mathrm{COM}) = \frac{\sum_{i=1}^{n}(\mathrm{COM})_i}{n}, \tag{C9}$$

$$\sigma(\mathrm{COM}) = \sqrt{\frac{\sum_{i=1}^{n}[(\mathrm{COM})_i - \mu(\mathrm{COM})]^2}{n-1}}. \tag{C10}$$

[46] The mean and standard deviation of TM are given by

$$\mu(\mathrm{TM}) = \frac{\sum_{i=1}^{n}(\mathrm{TM})_i}{n}, \tag{C11}$$

$$\sigma(\mathrm{TM}) = \sqrt{\frac{\sum_{i=1}^{n}[(\mathrm{TM})_i - \mu(\mathrm{TM})]^2}{n-1}}. \tag{C12}$$

Notation

x, y horizontal and vertical spatial coordinates, respectively [L].
$\Delta x, \Delta y$ horizontal and vertical element sizes, respectively [L].
ΔL transport distance between two sides of an element measured in the direction of groundwater flow [L].
H, L depth and length of a model, respectively [L].
k permeability of a porous medium [L^2].
g gravitational acceleration [LT^{-2}].
μ dynamic viscosity [$ML^{-1}\ T^{-1}$].
ε effective porosity [–].
ρ_0 base reference fluid density [ML^{-3}].
ρ fluid density [ML^{-3}].
$\Delta\rho$ density difference between maximum density and base reference density [ML^{-3}].
$\overline{\alpha}$ density difference ratio of density difference to base reference density [–].
S_s specific storage [L^{-1}].
m mass flux across the source boundary [$L^3\ T^{-1}$].
W width of the source zone equal to unity for the cross-sectional layout of the domain [L].
L_s length scale of the source zone [L].
C_0 normalized base reference concentration [–].
C normalized fluid concentration [–].
C_s normalized maximum concentration [–].
ΔC maximum concentration difference between base reference concentration and maximum concentration.
C_{node} normalized concentration of a node at the top boundary [–].
C_{dense} normalized concentration of dense water [–].
rand (0) a random function used for generating fractions uniformly distributed between 0 and 1 [–].
Q_ρ fluid mass source/sink [T^{-1}].
Q_c solute mass source/sink [$ML^{-3}\ T^{-1}$].
j Fickian mass flux [$ML^{-2}\ T^{-1}$].
$\mathbf{v}$ pore (intrinsic) velocity [LT^{-1}].
p fluid pressure [$ML^{-1}\ T^{-2}$].
Ra nondimensional Rayleigh number [–].
D_0 molecular diffusion coefficient [$L^2\ T^{-1}$].
β_L longitudinal dispersivity [L].
β_T transverse dispersivity [T].
Pe mesh PECLET number [–].
$\boldsymbol{I}$ unit (identity) tensor [–].
n number of samples in a set of models [–].
Sh Sherwood number [–].
TM total solute mass [ML^{-3}].
DPF deepest plume front [L].
COM vertical center of solute mass [L].
NOF number of fingers [–].
$\mu(Sh)$ mean of Sh [–].
$\sigma(Sh)$ standard deviation of Sh [–].
μ(TM) mean of TM [–].
σ(TM) standard deviation of TM [–].
μ(DPF) mean of DPF [L].
σ(DPF) standard deviation of DPF [L].
μ(COM) mean of COM [L].
σ(COM) standard deviation of COM [L].
μ(NOF) mean of NOF [–].
σ(NOF) standard deviation of NOF [–].

[47] **Acknowledgments.** Author Y. Xie wishes to acknowledge the financial support provided by a CSC living-stipend scholarship of Chinese Government, a fee-waiver scholarship from Flinders University, and a scholarship from the National Centre for Groundwater Research and Training for the postgraduate study. Mario Putti and two other anonymous reviewers are gratefully appreciated for constructive comments to strengthen the quality of the manuscript. This work was funded by the National Centre for Groundwater Research and Training, a collaborative initiative of the Australian Research Council and the National Water Commission.

References

Ackerer, P., A. Younes, and R. Mose (1999), Modeling variable density flow and solute transport in porous medium: 1. Numerical model and verification, *Transp. Porous Media*, *35*(3), 345–373.
Bachmat, Y., and D. E. Elrick (1970), Hydrodynamic instability of miscible fluids in a vertical porous column, *Water Resour. Res.*, *6*(1), 156–171.
Cheng, P. (1978), Heat transfer in geothermal systems, *Adv. Heat Transfer*, *14*, 1–105.
Combarnous, M. A., and S. A. Bories (1975), Hydrothermal convection in saturated porous media, *Adv. Hydrosci.*, *10*, 231–307.
Diersch, H. J. G., and O. Kolditz (1998), Coupled groundwater flow and transport: 2. Thermohaline and 3D convection systems, *Adv. Water Resour.*, *21*(5), 401–425.
Diersch, H. J. G., and O. Kolditz (2002), Variable-density flow and transport in porous media: Approaches and challenges, *Adv. Water Resour.*, *25*, 899–944.
Elder, J. W. (1967), Transient convection in a porous medium, *J. Fluid. Mech.*, *27*(3), 609–623.
Freeze, R. A., and J. A. Cherry (1979), *Groundwater*, Prentice-Hall, Englewood Cliffs, NJ.
Frolkovic, P., and H. De Schepper (2001), Numerical modelling of convection dominated transport coupled with density driven flow in porous media, *Adv. Water Resour.*, *24*(1), 63–72.
Graf., T., and L. Degener (2011), Grid convergence of variable-density flow simulations in discretely-fractured porous media, *Adv. Water Resour.*, *34*, 760–769.
Han, W. S., S.-Y. Lee, C. Lu, and B. J. McPherson (2010), Effects of permeability on CO_2 trapping mechanisms and buoyancy-driven CO_2 migration in saline formations, *Water Resour. Res.*, *46*, W07510, doi:10.1029/2009WR007850.
Horne, R. N., and J. Caltagirone (1980), On the evolution of thermal disturbances during natural convection in a porous medium, *J. Fluid. Mech.*, *100*(2), 385–395.
Horton, C. W., and F. T. Rogers (1945), Convection currents in a porous medium, *J. Appl. Phys.*, *16*, 367–370.
Illangasekare, T., et al. (2006), Impacts of the 2004 tsunami on groundwater resources in Sri Lanka, *Water Resour. Res.*, *42*(5), W05201, doi:10.1029/2006WR004876.
Jensen, R. V. (1987), Classical chaos, *Am. Sci.*, *75*, 168–181.
Johannsen, K. (2003), On the validity of the Boussinesq approximation for the Elder problem, *Comput. Geosci.*, *7*(3), 169–182.
Kolditz, O., and H. J. Diersch (1993), Quasi-steady-state strategy for numerical simulation of geothermal circulation in hot dry rock fractures, *Int. J. Non-Lin. Mech.*, *28*(4), 467–481.
Kolditz, O., R. Ratke, H. J. G. Diersch, and W. Zielke (1998), Coupled groundwater flow and transport: 1. Verification of variable-density flow and transport models, *Adv. Water Resour.*, *21*, 27–46.
Kooi, H., J. Groen, and A. Leijnse (2000), Modes of seawater intrusion during transgressions, *Water Resour. Res.*, *36*(12), 3581–3589.
Kreyszig, E. (1988), *Advanced Engineering Mathematics*, 6th ed., John Wiley, New York.
Lapwood, E. R. (1948), Convection of a fluid in a porous medium, *Math. Proc. Cambridge Philos. Soc.*, *44*(04), 508–521.
Larocque, M., P. G. Cook, K. Haaken, and C. T. Simmons (2009), Estimating flow using tracers and hydraulics in synthetic heterogeneous aquifers, *Ground Water*, *47*(6), 786–796.
Mazzia, A., L. Bergamaschi, and M. Putti (2001), On the reliability of numerical solutions of brine transport in groundwater: Analysis of infiltration from a salt lake, *Transp. Porous Media*, *43*(1), 65–86.

Nield, D. A., and C. T. Simmons (2007), A discussion on the effect of heterogeneity on the onset of convection in a porous medium, *Transp. Porous Media*, *68*, 413–421.

Oldenburg, C. M., and K. Pruess (1995), Dispersive transport dynamics in a strongly coupled groundwater-brine flow system, *Water Resour. Res.*, *31*(2), 289–302.

Post, V. E. A., and H. Kooi (2003), Rates of salinization by free convection in high-permeability sediments: Insights from numerical modeling and application to the Dutch coastal area, *Hydrogeol. J.*, *11*, 549–559.

Post, V. E. A., and C. T. Simmons (2010), Free convective controls on sequestration of salts into low-permeability strata: Insights from sand tank laboratory experiments and numerical modelling, *Hydrogeol. J.*, *18*(1), 39–54, doi:10.1007/s10040-009-0521-4.

Prasad, A., and C. T. Simmons (2003), Unstable density-driven flow in heterogeneous porous media: A stochastic study of the Elder [1967b] "short heater" problem, *Water Resour. Res.*, *39*(1), 1007, doi:10.1029/2002WR001290.

Prasad, A., and C. T. Simmons (2005), Using quantitative indicators to evaluate results from variable-density groundwater flow models, *Hydrogeol. J.*, *13*, 905–914.

Renard, P. (2005), The future of hydraulic tests, *Hydrogeol. J.*, *13*(1), 259–262.

Schincariol, R. A. (1998), Dispersive mixing dynamics of dense miscible plumes: Natural perturbation initiation by local-scale heterogeneities, *J. Contam. Hydrol.*, *34*, 247–271.

Schincariol, R. A., and F. W. Schwartz (1990), An experimental investigation of variable density flow and mixing in homogeneous and heterogeneous media, *Water Resour. Res.*, *26*(10), 2317–2329.

Schincariol, R. A., F. W. Schwartz, and C. A. Mendoza (1994), On the generation of instabilities in variable density flow, *Water Resour. Res.*, *30*(4), 913–927.

Simmons, C. T. (2005), Variable density groundwater flow: From current challenges to future possibilities, *Hydrogeol. J.*, *13*(1), 116–119.

Simmons, C. T., and K. A. Narayan (1997), Mixed convection processes below a saline disposal basin, *J. Hydrol.*, *194*, 263–285.

Simmons, C. T., and K. A. Narayan (1998), Modelling density-dependent flow and solute transport at the Lake Tutchewop saline disposal complex, Victoria, *J. Hydrol.*, *206*(3–4), 219–236.

Simmons, C. T., K. A. Narayan, and R. A. Wooding (1999), On a test case for density-dependent groundwater flow and solute transport models: The salt lake problem, *Water Resour. Res.*, *35*(12), 3607–3620.

Simmons, C. T., T. R. Fenstemaker, and J. M. Sharp (2001), Variable-density groundwater flow and solute transport in heterogeneous porous media: Approaches, resolutions and future challenges, *J. Contam. Hydrol.*, *52*(1–4), 245–275.

Simmons, C. T., K. A. Narayan, J. A. Woods, and A. L. Herczeg (2002), Groundwater flow and solute transport at the Mourquong saline-water disposal basin, Murray Basin, southeastern Australia, *Hydrogeol. J.*, *10*(2), 278–295.

Simmons, C. T., A. V. Kuznetsov, and D. A. Nield (2010), Effect of strong heterogeneity on the onset of convection in a porous medium: Importance of spatial dimensionality and geologic controls, *Water Resour. Res.*, *46*, W09539, doi:10.1029/2009WR008606.

Van Dam, R. L., C. T. Simmons, D. W. Hyndman, and W. W. Wood (2009), Natural free convection in porous media: First field documentation in groundwater, *Geophys. Res. Lett.*, *36*, L11403, doi:10.1029/2008GL036906.

van Reeuwijk, M., S. A. Mathias, C. T. Simmons, and J. D. Ward (2009), Insights from a pseudospectral approach to the Elder problem, *Water Resour. Res.*, *45*, W04416, doi:10.1029/2008WR007421.

Voss, C. I., and W. R. Souza (1987), Variable density flow and solute transport simulation of regional aquifers containing a narrow freshwater-saltwater transition zone, *Water Resour. Res.*, *23*(10), 1851–1866.

Wooding, R. A. (2007), Variable-density saturated flow with modified Darcy's law: The salt lake problem and circulation, *Water Resour. Res.*, *43*, W02429, doi:10.1029/2005WR004377.

Wooding, R. A., S. W. Tyler, and I. White (1997), Convection in groundwater below an evaporating salt lake: 1. Onset of instability, *Water Resour. Res.*, *33*(6), 1199–1217.

Woods, J. A., and G. F. Carey (2007), Upwelling and downwelling behavior in the Elder-Voss-Souza benchmark, *Water Resour. Res.*, *43*, W12403, doi:10.1029/2006WR004918.

Xie, Y., C. T. Simmons, A. D. Werner, and J. D. Ward (2010), Effect of transient solute loading on free convection in porous media, *Water Resour. Res.*, *46*, W11511, doi:10.1029/2010WR009314.

Xie, Y., C. T. Simmons, and A. D. Werner (2011), Speed of free convective fingering in porous media, *Water Resour. Res.*, *47*, W11501, doi:10.1029/2011WR010555.

Zhang, H., and F. W. Schwartz (1995), Multispecies contaminant plumes in variable density flow systems, *Water Resour. Res.*, *31*(4), 837–847.

Zimmermann, S., P. Bauer, R. Held, W. Kinzelbach, and J. H. Walther (2006), Salt transport on islands in the Okavango Delta: Numerical investigations, *Adv. Water Resour.*, *29*, 11–29.

H.-J. G. Diersch, DHI-WASY Institute for Water Resources Planning and Systems Research, Watersdorfer Strasse 105, Berlin, Germany.

C. T. Simmons, A. D. Werner, and Y. Xie, National Centre for Groundwater Research and Training, Flinders University, GPO Box 2100, Adelaide, SA 5001, Australia. (yueqing.xie@flinders.edu.au)